TROPDAD: A New Ligand for the Synthesis of Water-Stable Paramagnetic [16 + 1]-Electron Rhodium and Iridium Complexes

Frank Breher,[a] Carsten Böhler,[a] Gilles Frison,[a] Jeffrey Harmer,[b] Lorenz Liesum,[b] Arthur Schweiger,*[b] and Hansjörg Grützmacher*[a]

Dedicated to Professor Gottfried Huttner on the occasion of his 66th birthday

Abstract: The new tetradentate ligand 1,4-bis(5 *H*-dibenzo[*a*,*d*]cyclohepten-5-yl)-1,4-diazabuta-1,3-diene (^{H}tropdad) allows the syntheses of the 16-electron cationic rhodium complexes [M(^{H}tropdad)](O_3SCF_3) (M = Rh, Ir). The structure of the rhodium complex was determined by X-ray analysis and points to a description of these as [M^{+1}(^{H}tropdad)^{0}] with short C=N bonds (av 1.285 Å) and a long C–C bond (1.46 Å) in the diazabutadiene (dad) moiety, that is the M → dad charge-transfer is negligible. Both [Rh(^{H}tropdad)]$^{+}$ and [Ir(^{H}tropdad)]$^{+}$ are reduced at very low potentials ($E^{1}_{1/2}$ = −0.56 V and $E^{1}_{1/2}$ = −0.35 V, respectively) which allowed the quantitative synthesis of the neutral paramagnetic complexes [M(^{H}tropdad)]^{0} (M = Rh, Ir) by reacting the cationic precursor complexes simply with zinc powder. The [M(^{H}tropdad)]^{0} complexes are stable against protic reagents in organic solvents. Continuous wave and pulse EPR spectroscopy was used to characterize the paramagnetic species and the hyperfine coupling constants were determined: [Rh(^{H}tropdad)]^{0}: A_{iso}(^{14}N) = 11.9 MHz, A_{iso}(^{1}H) = 14.3 MHz, A_{iso}(^{103}Rh) = −5.3 MHz; [Ir(^{H}tropdad)]^{0}: A_{iso}(^{14}N) = 11.9 MHz, A_{iso}(^{1}H) = 14.3 MHz. In combination with DFT calculations, the experimentally determined *g* and hyperfine matrices could be orientated within the molecular frame and the dominant spin density contributions were determined. These results clearly show that the complexes [M(^{H}tropdad)]^{0} are best described as [M^{+1}(^{H}tropdad)$^{\bullet-}$] with a [16 + 1] electron configuration.

Keywords: EPR spectroscopy · HYSCORE spectroscopy · iridium · N ligands · rhodium

Introduction

The resonance forms shown in Equation (1) can be used to approximate the electronic structure of a metal complex with a "non-innocent" ligand L.[1]

$$\underset{\mathbf{A}}{M(L)} \leftrightarrow \underset{\mathbf{B}}{M^{+}(L^{\bullet-})} \leftrightarrow \underset{\mathbf{C}}{M^{2+}(L^{2-})} \quad (1)$$

As "non-innocent" ligands L, chelates such as quinones Q and their diimine derivatives,[1a] N-heterocyclic chelates (NHchel), such as bipyridine or phenanthroline, and their derivatives,[1b–g] and 1,4-diazabutadienes (e.g., dad = RN=CR^{1}–CR^{1}=NR), are most frequently employed.[1h,i] These types of ligands contribute actively to the redox state of the complex. For some complexes even an internal electron-transfer equilibrium ("redox isomerism" or "valence tautomerism") of the type $M^{+}(L^{\bullet-}) \rightleftharpoons M^{2+}(L^{2-})$ has been established.[2] With respect to this work, the rhodium and iridium complexes **I**–**III** are especially relevant (Scheme 1).

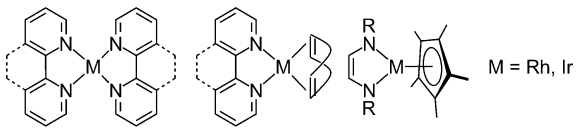

I **II** **III**

Scheme 1. Neutral rhodium and iridium complexes with *N*-heterocyclic chelates (NHchel) or 1,4-diazabutadiene (dad) as "non-innocent" ligands.

The neutral complexes of type **I** containing *formally* rhodium(0) or iridium(0) have been intensively studied by DeArmond and co-workers[1b–e] by electrochemical means but they were never obtained in monomeric form.[3] The electro-

[a] Prof. Dr. H. Grützmacher, Dr. F. Breher, Dr. C. Böhler, Dr. G. Frison
Laboratory of Inorganic Chemistry
ETH-Hönggerberg, 8093 Zürich (Switzerland)
Fax: (+41) 1 632 1032
E-mail: gruetzmacher@inorg.chem.ethz.ch

[b] Prof. Dr. A. Schweiger, Dr. J. Harmer, Dr. L. Liesum
Laboratory of Physical Chemistry
ETH-Hönggerberg, 8093 Zürich (Switzerland)
Fax: (+41) 1 632 1021
E-mail: schweiger@phys.chem.ethz.ch

Supporting information for this article is available on the WWW under http://www.chemeurj.org or from the author.

 DOI: 10.1002/chem.200204700

chemistry of mixed *N*-heterocyclic olefin complexes of type **II** was also studied, but the complexes were not isolated to our knowledge.[1f,g] Kaim and co-workers studied the irreversible (ECE mechanism) two-electron reduction of the complexes, $[Cp^*MCl(dad)]^+ + 2e^- \rightarrow [Cp^*M(dad)]$ (**III**) $+ Cl^-$ (M = Rh, Ir), and isolated the complexes **III**.[4] The reduction of the non-innocent $[dad]^0$ ligand to its 1,2-diamidoethylene form $[dad]^{2-}$ was unambiguously demonstrated in these cases.

An interesting property of the cited rhodium and iridium complexes is that their reduction potentials are relatively low. Using the tropp ligand (see inset in Scheme 2 below), we isolated the first examples of stable low-valent tetracoordinate Rh^0 and Ir^0 complexes[5a,b] which were characterized by pulse EPR spectroscopy.[5c] The interpretation of these results led us to conclude that the unpaired electron is predominantly located on the metal center in the corresponding $[M(tropp)_2]^0$ complexes (M = Co-Ir). We wondered whether we could also employ the tropylidenyl unit, trop, for the synthesis of stable *formally* zerovalent rhodium and iridium complexes in which a 1,4-*dia*zabuta*d*iene (dad) unit[1h,g] was an archetype of a "non-innocent" ligand. Herein we report: 1) the first examples of isolated neutral mononuclear paramagnetic rhodium and iridium dad complexes which are best represented by the resonance form **B** in Equation (1), and 2) a detailed investigation of these compounds by continuous wave (CW) and pulse EPR spectroscopy. Remarkably, the new ligand tropdad, which we report here, allows the synthesis of complexes whose reduction potentials are sufficiently low to make them stable against protic solvents.

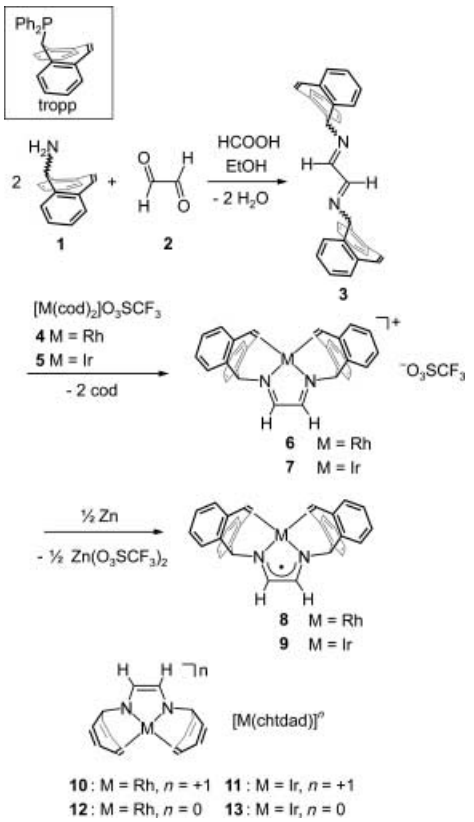

Scheme 2. Synthesis of the ligand ^{H}tropdad (**3**) and the $[M(tropdad)]^n$ complexes **6**–**9** (M = Rh, Ir; $n = +1, 0$), DFT-calculated $[M(chtdad)]^n$ complexes **10**–**13**.

Results

Syntheses: We synthesized compound **3** (Scheme 2) to use as a ligand. It contains both, a trop unit, which we have found useful in the synthesis of stable low-valent Rh and Ir complexes, and a diazadiene moiety. This potentially tetradentate ligand, named hereafter ^{H}tropdad [IUPAC: 1,4-bis(5*H*-dibenzo[*a*,*d*]cyclohepten-5-yl)-1,4-diazabuta-1,3-diene], is readily obtained in excellent yields by a condensation reaction of tropamine **1** [IUPAC: (5*H*-dibenzo[a,d]cyclohepten-5-yl)amine] with glyoxal **2** (Scheme 2).[6]

In most organic solvents, **3** is almost insoluble, however, upon reaction with the complexes $[M(cod)_2]O_3SCF_3$ (**4**: M = Rh; **5**: M = Ir; cod = η^4-1,5-cyclooctadiene) in THF, deep red solutions are obtained from which the 16-electron ^{H}tropdad complexes **6** and **7**, respectively, can be precipitated as intense red crystals in almost quantitative yields. The structure of the rhodium complex **6** determined by X-ray diffraction[7] is shown in Figure 1.[8]

In this almost perfect C_{2v}-symmetric structure, the ^{H}tropdad acts as a tetradentate ligand and wraps around the rhodium atom preventing any intermolecular stacking.[3] This is nicely demonstrated by the view of the molecule given in Figure 1 (top). Note that ^{H}tropdad offers a remarkably rigid coordination sphere containing no rotating groups. Two conjugated π systems, that is the dad unit and the C=C bonds of the trop units, are arranged in an almost perfect perpendicular fashion (N1-Ct-C4 89.4°, N1-Ct-C5 90.6°; Ct = midpoint of the C4=C5

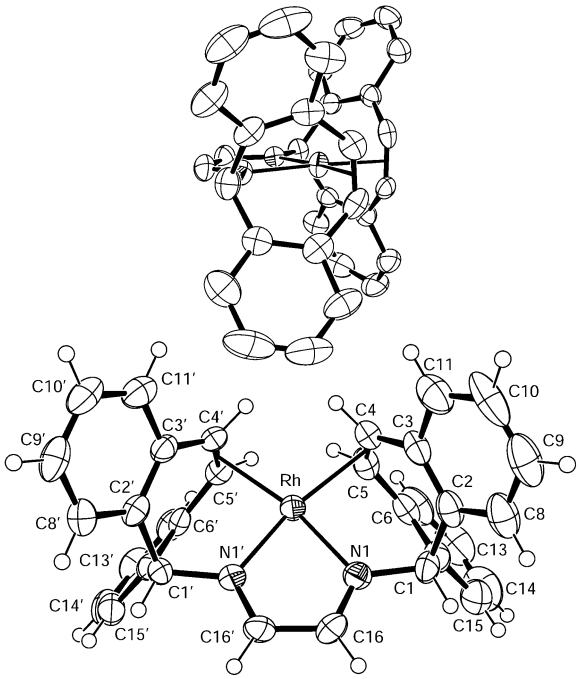

Figure 1. Molecular structure and numbering scheme for compound **6**; thermal ellipsoids are drawn at the 50% probability level. The atoms of the counterion (OTf^-) are omitted for clarity; hydrogen atoms are drawn with arbitrary radii; selected bond lengths [Å] and angles [°]: Rh–N1 2.025(5), Rh–N1′ 2.012(5), Rh–C4 2.185(7), Rh–C4′ 2.185(6), Rh–C5 2.199(7), Rh–C5′ 2.182(6), N1–C16 1.289(9), N1′–C16′ 1.281(8), C16–C16′ 1.46(1), N1–C1 1.455(9), N1′–C1′ 1.486(8), C4–C5 1.38(1), C4′–C5′ 1.39(1); N1-Rh-N1′ 78.9(2), N1-Rh-C4 90.0(3), N1-Rh-C5 90.2(2), N1′-Rh-C4′ 90.6(2), N1′-Rh-C5′ 90.4(2), C4-Rh-C4′ 92.6(2), C5-Rh-C5′ 94.7(3).

bond). Selected structural parameters of **6** are listed in Table 1 together with calculated values of the model complexes $[M(chtdad)]^n$ **10**–**13** (Scheme 2; chtdad = 1,4-bis(*cyclo*hepta-*t*rienyl)-1,4-*diaz*abuta*d*iene).

Table 1. Selected experimental bond lengths [Å] for **6** and calculated values (DFT) for **10**—**13**, and calculated NBO charges (DFT) for **10**–**13**. C–C_{dad} denotes the C–C bond in the diazadiene moiety and C=C_{trop} denotes the metal-coordinated C=C double bond.

	Metal	*n*	M–N	C=N	C–C_{dad}	C=C_{trop}
6[a]	Rh	+1	2.025, 2.012	1.289, 1.281	1.46	1.38, 1.39
10	Rh	+1	2.030	1.291	1.453	1.409
11	Ir	+1	2.017	1.298	1.445	1.423
12	Rh	0	2.015	1.334	1.400	1.409
13	Ir	0	2.005	1.336	1.400	1.445
			NBO charges (DFT)			
	Metal	*n*	*q*(Metal)	*q*(N)	*q*(C–C_{dad})	*q*(C=C_{trop})
10	Rh	+1	+0.43	−0.39	+0.64	−0.57
11	Ir	+1	+0.52	−0.41	+0.64	−0.62
12	Rh	0	+0.45	−0.50	+0.36	−0.62
13	Ir	0	+0.58	−0.52	+0.40	−0.69

[a] values in **6**: Rh–N1, Rh–N1′; C1=N1, C1′=N1′; C16=C16′; C4=C5, C4′=C5′.

The experimental data for **6** agree well with the calculated values for **10** and leave no doubt about the assignment of the formal oxidation states as $Rh^+(^Htropdad^0)$.[4, 8] Indeed, in the ^1H NMR spectrum the N=CH–CH=N protons of the dad unit are shifted to higher frequencies ($\Delta\delta = \delta_{complex} - \delta_{free\ ligand}$); **6**: $\Delta\delta = 0.55$ ppm; **7**: $\Delta\delta = 1.66$ ppm) upon coordination of **3**, indicating that charge shifts from the dad unit to the metal, that is the dad unit serves as a donor and not as an acceptor. This shift is especially pronounced for the iridium complex **7**. On the contrary, shifts to lower frequencies are observed when the metal fragment serves as donor and charge is accumulated on the ligand.[4] This is the case for the olefinic protons of the CH=CH unit within the trop fragment which are shifted to lower frequencies, that is the coordination shifts $\Delta\delta$ become negative (**6**: $\Delta\delta = -1.46$ ppm; **7**: $\Delta\delta = -1.09$ ppm). This phenomenon indicates efficient metal-to-olefin back-bonding.

Both complexes, **6** and **7**, are (quasi)reversibly reduced to the neutral complexes **8** and **9**, respectively, at the lowest potentials reported to date for any 16-electron rhodium or iridium complex (**6**: $E^1_{1/2} = -0.56$ V; **7**: $E^1_{1/2} = -0.35$ V referenced versus the Fc/Fc^+ couple which has a potential of +0.352 V versus Ag/AgCl under our conditions). A superposition of the cyclic voltammograms obtained with **6** (solid line) and **7** (dotted line) in THF/0.1 M nBu_4NPF_6 as electrolyte is shown in Figure 2.

A second (quasi)reversible redox wave is observed for the process $[M(^Htropdad)]^0 + e^- \rightarrow [M(^Htropdad)]^-$ (M = Rh, Ir) at $E^2_{1/2} = -1.29$ V (**8**) and $E^2_{1/2} = -1.10$ V (**9**), respectively. The disproportionation constants K_{disp} for the reaction $2\,[M(^Htropdad)]^0 \rightleftharpoons [M(^Htropdad)]^+ + [M(^Htropdad)]^-$ are calculated to be 4.6×10^{-13} for M = Rh and 2.1×10^{-13} for M = Ir, and are 5 to 6 orders of magnitude smaller than for the comparable $[M(tropp^{ph})_2]^{+1/0/-1}$ complexes.[5] This observation indicates the high thermodynamic stability of the new

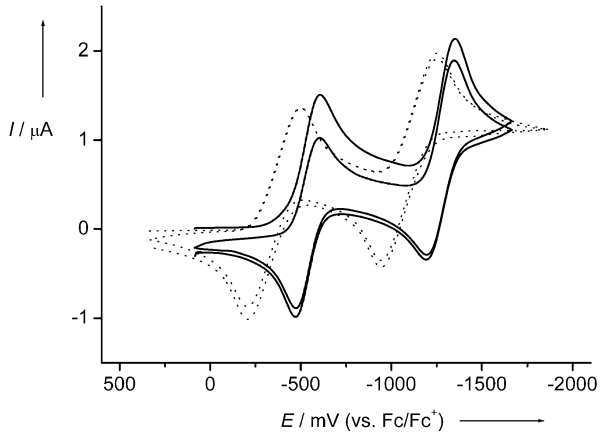

Figure 2. Cyclic voltammetry of **6** (solid line) and **7** (dotted line) at room temperature in THF. Scan rate 100 mV s^{-1}, Pt/nBu_4NPF_6/Ag.

$[M(^Htropdad)]^0$ complexes. Chemically, the reduced 17-electron complexes **8** and **9** can simply be prepared in quantitative yields by stirring a solution of the cationic precursors in THF with zinc powder. Unfortunately, all attempts to grow single crystals suitable for an X-ray analysis failed. Although a wide variety of different solvents and crystallization conditions were tried, only microcrystalline powders were obtained.

EPR spectroscopy: Information about the electronic structure of **8** and **9** was obtained from CW and pulse EPR spectroscopy, that is EPR spectroscopy at various microwave frequencies (X-, Q-, and W-band), pulse ENDOR (electron nuclear double resonance), and HYSCORE (hyperfine sublevel correlation) spectroscopy.[9] These investigations were combined with DFT calculations.[10] The *g* values as well as the metal, nitrogen, and proton hyperfine couplings for the rhodium and iridium complexes are listed in Table 2. The calculated hyperfine couplings for the model complexes $[M(chtdad)]^0$ **12** (M = Rh) and **13** (M = Ir) are also given.

The CW EPR spectra of **8** in THF at 298 K (a), 120 K (b), and 77 K (c), and of **9** at 120 K (d) are shown in Figure 3, together with the corresponding simulated spectra. The small anisotropy of the axial *g* matrix of **8** is resolved only in the frozen solution spectra at Q- and W-band (see insets of Figure 4 for the spectrum at Q-band). The solution spectrum of **9** exhibits a single broad line with no resolved hyperfine structure (not shown).

The anisotropic hyperfine interactions of the nitrogens, rhodium, and protons in **8** and **9** were obtained from orientation-selective HYSCORE and ENDOR spectra at Q- and X-band. Two representative Q-band HYSCORE spectra of **8** are shown in Figure 4.

Figure 4a shows the Q-band HYSCORE spectrum obtained when orientations close to $g_\perp$ are selected. Since the nitrogens are strongly coupled, the cross-peaks representing the correlations of the nuclear frequencies in the two electron spin manifolds are predominately in the second quadrant.[9] The hyperfine coupling is found to be strongly anisotropic ($A_x = 0.9$ MHz, $A_y = 34$ MHz) which is manifested by two long ridges (red double arrow). Cross-peaks assigned to rhodium ($A_x = -10$ MHz, $A_y = -12$ MHz) are also labeled (yellow arrows). In the spectrum shown in Figure 4b only orientations

Table 2. Experimental hyperfine coupling constants [MHz] of the [M(^{H}tropdad)] complexes **8** and **9** and calculated values of the [M(chtdad)] (M = Rh, Ir) complexes **12** and **13**.[a]

	Experimental [Rh(^{H}tropdad)] (**8**)					DFT [Rh(chtdad)] (**12**)				
nuclei	A_{iso}	A_x	A_y	A_z	β_{exp}[c]	A_{iso}	A_x	A_y	A_z	β_{DFT}[d]
^{14}N[b]	11.9	0.9	34	0.9		17.7	4.8	43.8	4.6	
^{1}H[b]	14.3	22.5	15.3	5.0	±41°	−15.4	−23.0	−18.4	−4.8	±41°
^{103}Rh	−5.3	−10.0	−12.0	6.0		0.00	−0.04	−0.01	0.05	
	Experimental [Ir(^{H}tropdad)] (**9**)					DFT [Ir(chtdad)] (**13**)				
^{14}N[b]	11.9	0.9	34.0	0.9		15.5	3.9	39.2	3.5	
^{1}H[b]	14.3	22.5	15.3	5.0	±41°	−15.7	−23.4	−18.6	−5.2	±41°

[a] g values **8**: $g_{iso}=2.0022$, $g_x=g_y=g_\perp=1.9977$, $g_z=g_\parallel=2.0113$. **9**: $g_{iso}=2.0024$, $g_x=g_y=g_\perp=1.9870$, $g_z=g_\parallel=2.0332$. DFT spin densities: **12**: ρ(N) = 29.5 % (×2), ρ(C-C$_{dad}$) = 16.1 % (×2), ρ(C=C$_{trop}$) = 2.1 % (×4). **13**: ρ(N) = 26.3 % (×2), ρ(C–C$_{dad}$) = 16.6 % (×2), ρ(C=C$_{trop}$) = 3.2 % (×4). [b] Absolute values are given for the experimental data. Estimated error of ±1 MHz. [c] Angle β_{exp} defines a rotation of the $\mathbf{A}_x$ axis (from $\mathbf{g}_x$) around the $\mathbf{g}_y$ axis. [d] Angle β_{DFT} defines a rotation of the $\mathbf{A}_x$ axis (from x) around the y axis.

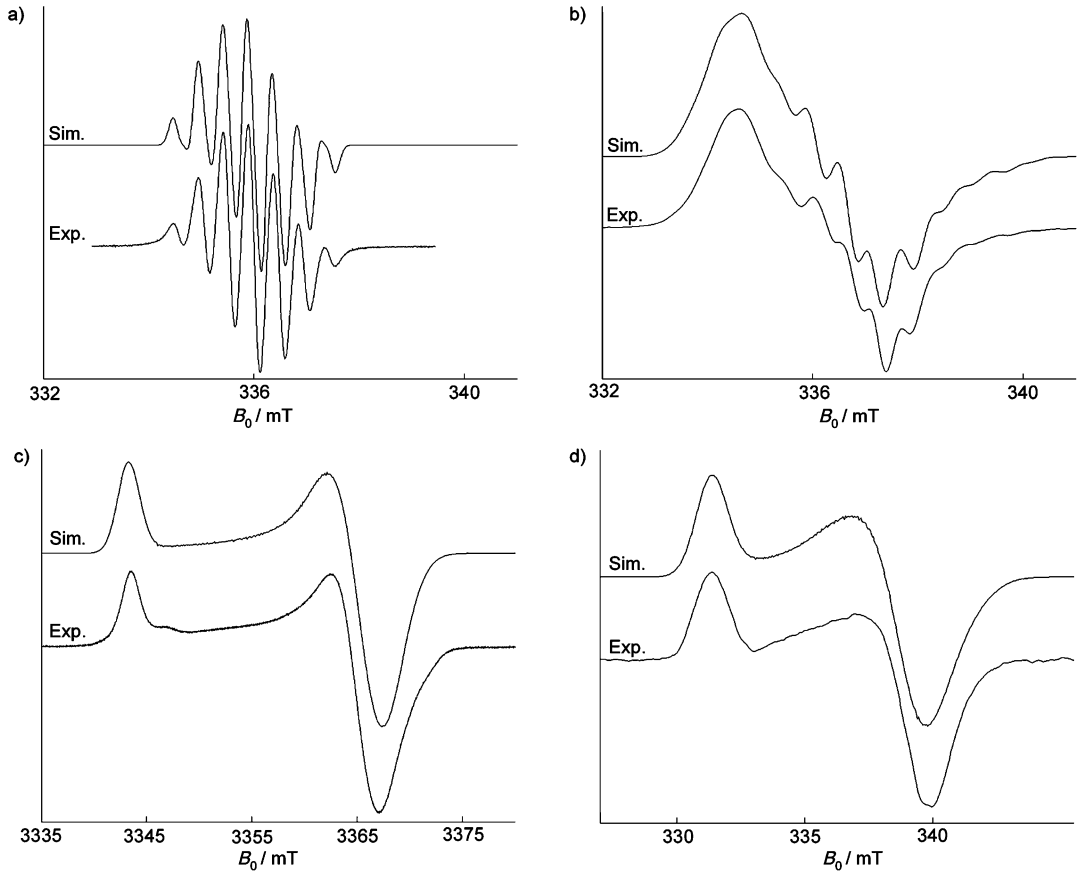

Figure 3. Experimental (Exp.) and simulated (Sim.) CW EPR spectra of **8** in THF: a) at room temperature at X-band, b) at 120 K at X-band, c) at 77 K at the W-band, and d) of **9** at 120 K at the X-band.

close to $g_\parallel$ are observed. In this single-crystal like spectrum, a small nitrogen ($A_z = 0.9$ MHz, red arrows) and rhodium ($A_z =$ 6 MHz, yellow arrows) interaction is found. The HYSCORE spectra of **9** (not shown) exhibit virtually the same nitrogen signals. In accord with the above assignment, none of the signals assigned to rhodium in the spectrum of **8** are observed in the spectrum of **9**.

Additional information used to assign the rhodium signals was obtained from a hyperfine-decoupling experiment using the two-pulse spin-locked ESEEM sequence.[11]

In this 2D experiment the ESEEM frequencies ν_{ESEEM} are correlated to the hyperfine-decoupled nuclear frequencies ν_{dec}, which for an $I = ½$ nucleus and a sufficently large decoupling field approach the nuclear Larmor frequency ν_I of the corresponding nucleus. Figure 5 shows the spectrum for complex **8** obtained at an observer position close to $g_\perp$. The peaks at about 4.8 MHz and 11 MHz along the ESEEM dimension are assigned to rhodium, since they are correlated to the Larmor frequency of rhodium ($\nu_{Rh} = 1.7$ MHz) along the decoupling dimension. These data confirm the assignment of the rhodium peaks at 4.8 MHz in the HYSCORE spectrum. Satisfactory simulation of the Rh signals of the HYSCORE spectra and agreement with the isotropic hyperfine value determined from the CW solution spectrum was achieved

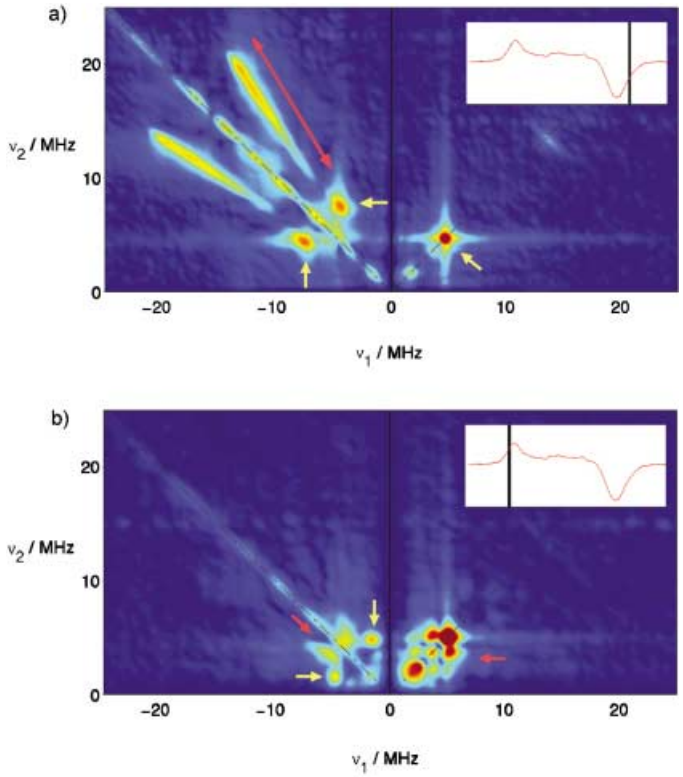

Figure 4. Q-band HYSCORE spectra of the rhodium complex **8** recorded at 20 K in THF. Orientations close to $g_\perp$ (a) and $g_\parallel$ (b) are selected. The red arrows [(a) and (b)] indicate the large anisotropy of the ^{14}N coupling. The yellow arrows indicate the rhodium peaks. Inset: Q-band CW EPR spectra with corresponding observer positions.

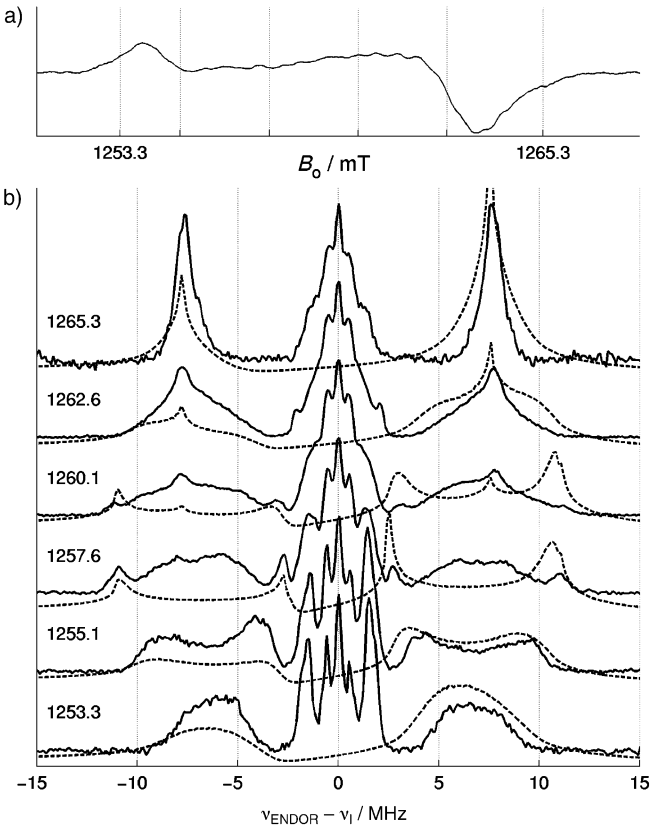

Figure 6. Q-band ^1H Davies–ENDOR spectra of the rhodium complex **8** recorded at 20 K in THF at different observer positions. a) FID-detected EPR spectrum (1st derivative) with the selected field positions, b) corresponding ENDOR spectra and simulations (dashed lines).

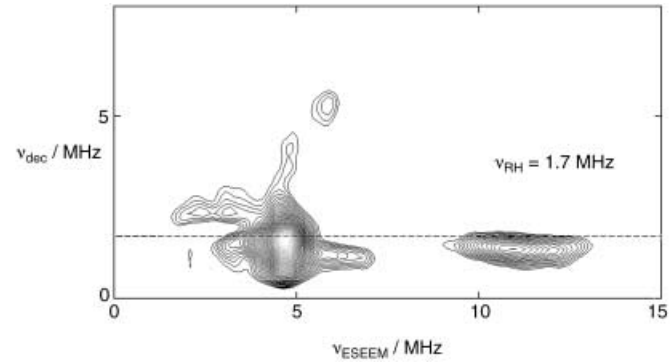

Figure 5. Q-band hyperfine-decoupling experiment of the rhodium complex **8** recorded at 20 K in THF at an observer position close to $g_\perp$.

with principal values of −10, −12, and 6 MHz. The Rh hyperfine matrix can be split into an isotropic part (A_{iso} = −5.3 MHz) and a dipolar part with principal values of −6.7, −4.7, and 11.4 MHz (the g_n value of Rh is negative and positive spin density was assumed). The anisotropic part is mainly due to a d-orbital contribution, with the value of 11.4 MHz pointing along the $\mathbf{A}_z$ axis and being collinear with $\mathbf{g}_\parallel$. These data highlight the influence of the Rh nucleus in determining the *g* matrix.

ENDOR spectra used to determine the proton hyperfine couplings for **8** are given in Figure 6 (the spectra for **9** are given in the Supporting Information). The simulations (dashed lines) were achieved with non-coaxial **g** and **A** matrices with the hyperfine $\mathbf{A}_x$ axes of H16′ and H16 rotated by $\beta_{exp} = \pm 41^\circ$ around the $\mathbf{g}_y$ axis, respectively.

The DFT calculations allow the experimentally determined **g** and hyperfine matrices to be orientated within the molecular frame. Calculations for nitrogen N1 and N1′ show that the $\mathbf{A}_y$ axis (largest hyperfine value) points in the *y* direction defined in Figure 7a , thus $\mathbf{g}_y$ is parallel to *y* (see Table 2). The $\mathbf{g}_x$ and $\mathbf{g}_z$ axes orientations can be inferred from the H16′ and H16 hyperfine matrices. DFT data orientate the $\mathbf{A}_x$ axes of H16′ and H16 in the *xz* plane with $\mathbf{A}_x$ rotated around the *y* axis by $\beta_{DFT} = +41^\circ$ and $\beta_{DFT} = -41^\circ$, respectively. Satisfactory simulations of the experimental data (Figure 6) were indeed achieved by rotating $\mathbf{A}_x$ (from $\mathbf{g}_x$) around $\mathbf{g}_y$ by $\beta_{exp} = \pm 41^\circ$, so that $\mathbf{g}_x$ is parallel to X and $\mathbf{g}_z$ is parallel to *z*.

Noteworthy, the DFT calculations on the model complexes [M(chtdad)] **12**, **13** do not reproduce the experimentally determined metal hyperfine couplings, while the agreement between the experimental and calculated data is very satisfactory for the nonmetal nuclei. A comparison of Figure 7b and 7c shows, that the SOMO (Figure 7b) reflects essentially the spin density distribution and both are localized on the N–C–C–N unit of the ligand. A very small negative spin density (−0.019 and −0.027, respectively) is calculated for the metal centers in **12** and **13** (grey shaded isosurface in Figure 7c).

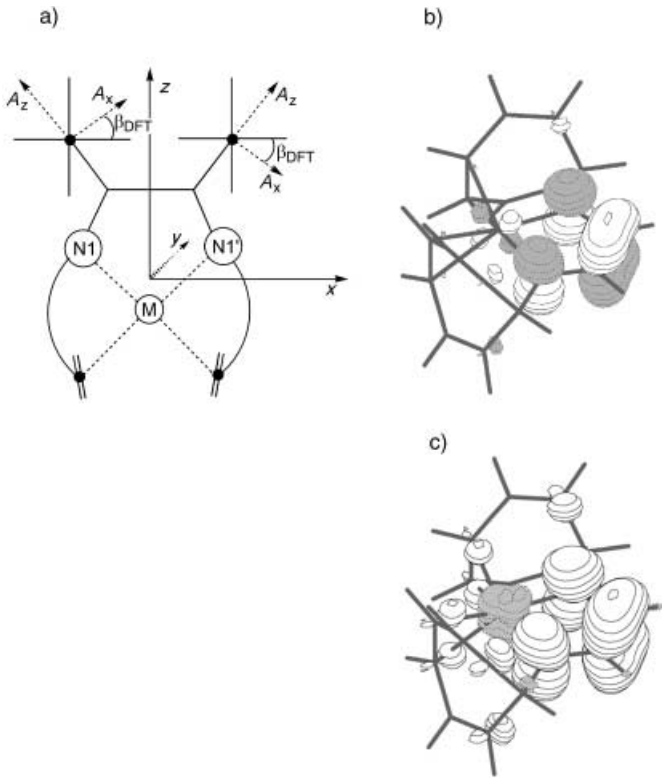

Figure 7. a) Schematic representation of the orientation of the *x*, *y*, and *z* axes and the ^{1}H hyperfine principal axes of H16 and H16′ calculated by DFT. b) SOMO calculated by DFT. Note that there is an excellent agreement between the DFT and experimentally determined ligand contributions. c) Spin density distribution calculated by DFT.

Combining the results from the CW EPR, HYSCORE, and ENDOR experiments, the hyperfine couplings of nitrogens, protons, and rhodium were obtained. These hyperfine couplings and the isotropic *g* values (**8**: 2.0022; **9**: 2.0024) are typical for paramagnetic complexes in which the unpaired electron is located predominantly on the dad moiety.[4]

We used the nitrogen hyperfine matrix of **8** and **9** to estimate the spin density in the s and p orbitals of the nitrogen atoms by comparing the data with those computed for the free ion. A total spin density $\rho_{tot} = 45\,\%$ was found for the two nitrogens; about 1 % residing in the s orbitals (0.5 % each) and about 44 % (22 % each) in the p orbitals (estimated from the dipolar part of the hyperfine couplings). As discussed above, the DFT calculations agree with this finding and also show that the spin density distribution is not significantly influenced by the metal (see values given in footnote to Table 2).

Comparison of the computed NBO charges (see values listed in the bottom of Table 1) of the 16-electron complexes **10** and **11** with those of the 17-electron complexes **12** and **13** shows that neither the metal charges nor the charge on the coordinated olefin C=C$_{trop}$ of the trop unit are significantly influenced, whereas the negative charge on the nitrogens increases and the positive charge on the CH=CH$_{dad}$ bridge decreases. Consequently, the [M(^{H}tropdad)]^0 complexes **8, 9** (M = Rh, Ir) are best described by the Lewis structure [M$^+$(^{H}tropdad$^{\bullet-}$)] and their valence-electron configuration is assigned as [16 + 1].[1i] Importantly, **8** and **9** are stable in deoxygenated THF/H_2O for at least several days and no significant decrease of the EPR signal intensity was observed.

Conclusion

The new tetradentate ^{H}tropdad ligand lowers the reduction potentials of the 16-electron complexes [M(^{H}tropdad)]$^+$ (M = Rh, Ir) significantly when compared to those of related complexes such as [M(bipy)(cod)]$^+$ or [M(phen)(cod)]$^+$ (see **II** in Scheme 1). Importantly, the neutral paramagnetic complexes [M(^{H}tropdad)]^0 **8** (M = Rh) and **9** (M = Ir) can be quantitatively prepared by a mild and cheap reducing agent of zinc powder and are stable in deoxygenated THF/H_2O for at least several days (no significant decrease of the EPR signal intensity was observed). This will allow us to investigate the reactivity of an organic radical (here a dad$^{\bullet-}$ radical) coupled functionally to an unsaturated metal center, here a 16-electron rhodium or iridium center, even under protic conditions. Complexes **8** and **9** react cleanly with oxygen and nucleophiles. These reactions are currently under investigation.

We have applied high-resolution pulse EPR methods to determine experimentally the proton, nitrogen, and rhodium (for **8**) hyperfine couplings. By using this data in combination with DFT calculations we were able to determine the orientation of the **g** and hyperfine matrices within the molecular frame. This level of detail is frequently achieved in single-crystal work but is not that common in frozen solution studies due to the inherent low resolution. It is found that the axes of the largest principal value of the nitrogen hyperfine tensors ($A_y = 34$ MHz) point in the direction of the nitrogen p orbitals that are perpendicular to the central plane of the complex. The EPR data leave no doubt that the electronic structure is best described as [M$^+$(^{H}tropdad$^{\bullet-}$)] with the unpaired electron mainly located on the ligand. Accordingly, the rhodium couplings of **8** ($|A_{iso}| = 5.3$ MHz) are somewhat smaller than those determined for the mixed phosphine olefin complexes *cis*/*trans*-[Rh(tropp^{Ph})$_2$]^0 ($|A_{iso}| = 17$ MHz and 21 MHz, respectively).[5c] Although the rhodium hyperfine coupling (and presumably the spin density on the rhodium) is small in **8** there is a measurable influence on the **g** matrix which is axial and has an anisotropy larger than that typically observed in organic radicals. It must be noted that the hyperfine coupling constants of the rhodium are not satisfactorily reproduced by the DFT calculations, while the agreement for main group element nuclei is good.[12, 13] There is certainly a need to refine the theoretical methods further and we hope that this work will contribute to efforts in this direction.

Experimental Section

General: All manipulations were performed under an argon atmosphere. All solvents were dried and purified by using standard procedures and were freshly distilled under argon from sodium/benzophenone (THF), from sodium/diglyme/benzphenone (*n*-hexane), or calcium hydride (CH_2Cl_2) prior to use. Air-sensitive compounds were stored an weighed in a glove box (Braun MB 150 B-G system), and reactions on small scale were

performed directly in the glove box. NMR spectra were either recorded on an AMX-500, Avance DRX-400, Avance DPX-300, or Avance DPX-250 system. The chemical shifts are given as δ values and were referenced against tetramethylsilane (TMS) for ^{1}H and ^{13}C. Coupling constants J are given in Hz as positive values regardless of their real individual signs. The multiplicity of the signals is indicated as s, d, or m for singlets, doublets, or multiplets, respectively. The abbreviation br. is given for broadened signals. Quaternary carbon atoms are indicated as C_{quart}, aromatic units as CH_{ar} when not noted otherwise. IR spectra were measured with the ATR-technique on a Perkin-Elmer 2000 FT-IR spectrometer in the range from 4000 cm^{-1} to 550 cm^{-1} using a KBr beamsplitter. The intensity of the absorption band is indicated as w (weak), m (medium), and s (strong). The UV/Vis spectra were measured with a UV/Vis/NIR Lambda 19 spectrometer in 0.5 cm quartz cuvettes. Cyclic voltammetry measurements were perfomed with EG&G potentiostate model 362. Mass spectra were taken on a Finnigan MAT 95 in the FAB mode.

Syntheses of [Rh(^{H}tropdad)](SO$_3$CF$_3$) (6) and [Ir(^{H}tropdad)](SO$_3$CF$_3$) (7): A solution of [M(cod)$_2$]Otf (**4**: M = Rh; **5**: M = Ir) in CH_2Cl_2 (3 mL) was added dropwise at room temperature to a suspension of ^{H}tropdad **3** (0.109 g, 0.25 mmol) in CH_2Cl_2 (3 mL). Upon addition of the metal precursor the initially colorless mixture turned into a dark red solution, which was stirred for one hour. The reaction mixture was concentrated to about half of its volume, layered with *n*-hexane, and stored at −30 °C. After 12 h, the dark red, crystalline product was isolated, washed with *n*-hexane, and dried in vacuum to give the analytically pure complex.

6: Yield: 86 %. M.p. 271–276 °C (decomp). ^{1}H NMR (300 MHz, CD_2Cl_2, 298 K): δ = 8.40 (d, ^3J(Rh,H) = 3.0 Hz, 2H; N=CH), 7.59–6.91 (m, 16H; CH_{ar}), 5.94 (d, ^3J(Rh,H) = 1.7 Hz, 2H; CHN), 5.47 ppm (d, ^2J(Rh,H) = 1.4 Hz, 4H; C=CH); ^{13}C NMR (75 MHz, CD_2Cl_2, 298 K): δ = 165.5 (N=CH), 137.3 (C_{quart}), 134.3 (C_{quart}), 131.3, 130.7, 130.2, 129.7, 128.9, 128.6 (CH_{ar}), 85.3 (C=CH), 75.9 ppm (CHN); IR (golden gate): $\tilde{\nu}$ = 1484 m, 1428 w, 1397 w, 1289 m, 1253 s, 1222 m, 1160 m, 1142 m, 1027 s, 951 m, 807 m, 754 s, 703 m, 636 s, 625 cm^{-1} s; UV/Vis (THF): λ_{max} = 409, 280 nm; MS (FAB): *m*/*z* (%): 539 (25) [M^+ − OTf], 191 (85) [trop$^+$], 147 (100) [OTf$^+$]. **7**: Yield: 91 %. M.p. 283–288 °C (decomp). ^{1}H NMR (300 MHz, CD_2Cl_2, 298 K): δ = 9.51 (s, 2H; N=CH), 7.64–7.31 (m, 16H; CH_{ar}), 6.56 (s, 2H; CHN), 5.84 ppm (s, 4H; C=CH); ^{13}C NMR (75 MHz, $CDCl_3$, 298 K): δ = 171.1 (N=CH), 139.4 (C_{quart}), 133.5 (C_{quart}), 130.5, 129.2, 128.6 (CH_{ar}), 75.8 (CHN), 74.5 ppm (C=CH); IR (golden gate): $\tilde{\nu}$ = 1488 m, 1252 s, 1223 s, 1154 s, 1026 s, 951 m, 897 m, 806 m, 754 s, 635 s, 626 cm^{-1} s; UV/Vis (THF): λ_{max} = 405, 275 nm; MS (FAB): *m*/*z* (%): 629 (15) [M^+ − OTf], 191 (90) [trop$^+$], 147 (100) [OTf$^+$].

Syntheses of [Rh(^{H}tropdad)] (8) and [Ir(^{H}tropdad)] (9): The cationic complexes [M(^{H}tropdad)]OTf **6** or **7** (0.5 mmol) were dissolved in THF (5 mL). An excess (≈5 equiv) of activated zinc powder was added and the suspension was stirred for one hour at room temperature. The solution containing the rhodium complex **8** turned goldish red, whereas the solution containing the iridium complex **9** became dark green. The turbid solution was filtered, the residue washed with THF (ca. 1 mL) and subsequently the filtrate was concentrated to about half of its volume under vacuum. After the solution was layered with *n*-hexane and cooled to −30 °C, the paramagnetic, air-sensitive complex was isolated as an intensely colored powder, which was dried in vacuum and stored under argon.

8: Yield: 85 %. M.p. 201–204 °C (decomp). IR (golden gate): $\tilde{\nu}$ = 1473 m, 1436 w, 1375 w, 1289 m, 1255 s, 1201 m, 1008 s, 952 m, 807 m, 768 m, 616 cm^{-1} s; UV/Vis (THF): λ_{max} = 443 nm. **9**: Yield: 78 %. 234–237 °C (decomp). IR (golden gate): $\tilde{\nu}$ = 1587 w, 1478 m, 1412 m, 1267 m, 1251 m, 1223 s, 1113 s, 1063 m, 984 m, 856 m, 767 m, 756 s, 682 cm^{-1} s; UV/Vis (THF): λ_{max} = 449 nm.

EPR spectroscopy: Continuous wave (CW) electron paramagnetic resonance measurements were performed at X-band on a Bruker ESP300 spectrometer (microwave frequency 9.43 GHz) equipped with a liquid nitrogen cryostat and at W-band on a Bruker ESP680 (microwave frequency 94.2 GHz) equipped with a liquid Helium cryostat. The spectra at X-band (W-band) were measured with a modulation amplitude of 0.05 (0.1) mT and a modulation frequency of 100 kHz, and the field was calibrated by using 2,2-diphenyl-1-picrylhydrazyl (DPPH) with a g value of 2.0036. Hyperfine sublevel correlation (HYSCORE) experiments were carried out at Q-band at 20 K on a home-built instrument[14] (mw frequency 35.3 GHz) with the pulse sequence $\pi/2$-τ-$\pi/2$-t_1-π-t_2-$\pi/2$-τ-echo. The following parameters were used: mw pulses of length $t_{\pi/2}$ = 16 ns and t_π = 16 ns, starting times of 96 ns for t_1 and t_2, and time increment Δt = 12 ns. To increase the modulation depth, the second and third $\pi/2$ pulses were replaced by pulses of length 64 ns.[15] To minimize blind spots spectra were measured with τ values of 96 and 154 ns. The two-pulse spin-locked electron spin echo envelope modulation (ESEEM) experiment[11] used the pulse sequence $\pi/2$-τ-T-τ-echo, where time τ and the length of the decoupling pulse T were varied. The following parameters were used: $t_{\pi/2}$ = 12 ns, $\Delta\tau$ = 8 ns, T_0 = 24 ns, ΔT = 16 ns and an mw field strength of $\omega_1/2\pi$ = 20.83 MHz. Davies-ENDOR experiments[9] used the pulse sequence π-T-$\pi/2$-τ-π-τ-echo with t_π = 80 ns and a 10 µs rf pulse (π pulse for matrix ^{1}H nuclei) of variable frequency applied during the time interval T. CW EPR and HYSCORE simulations were calculated using the EasySpin package[16] and programs written in-house,[17] respectively.

Acknowledgements

This work was supported by the Swiss National Science Foundation. We thank the Haarmann&Reimer GmbH for a generous gift of chemicals. F. Breher gratefully acknowledges a grant provided by the Deutsche Forschungsgemeinschaft.

[1] There is an extensive literature on this topic and only a very limited selection of papers related to this work are cited here: Quinones: For a review see a) C. G. Pierpont, C. W. Lange, *Prog. Inorg. Chem.* **1994**, *41*, 331; electrochemical studies with *N*-heterocyclic chelate complexes; b) [Rh(bpy)$_2$] and [Rh(phen)$_2$] complexes: H. Căldăraru, K. DeArmond, K. W. Hanck, Y. Em. Sahini, *J. Am. Chem. Soc.* **1976**, *98*, 4455–4457, and references therein; [Ir(bipy)$_x$] complexes: c) J. L. Kahl, K. W. Hanck, K. DeArmond, *J. Phys. Chem.* **1978**, *82*, 540, and references therein; [Ir(phen)$_x$] complexes: d) J. L. Kahl, K. W. Hanck, K. DeArmond, *J. Phys. Chem.* **1979**, *83*, 2606, and references therein; e) J. L. Kahl, K. W. Hanck, K. DeArmond, *J. Phys. Chem.* **1979**, *83*, 2611, and references therein; [M(NHchel)(diene)]$^+$ complexes (M = Rh, Ir; NHchel = bipy, phen and derivatives, diene = cod, nbd): f) W. A. Fordyce, K. H. Pool, G. A. Crosby, *Inorg. Chem.* **1982**, *21*, 1027–1030, and references therein; [Ir(phen)(cod)]$^+$ complexes (M = Rh, Ir; NHchel = bipy, phen, and derivatives): g) G. Costa, C. Tavagnacco, G. Balducci, G. Mestoni, G. Zassinovich, *J. Elektroanal. Chem.* **1989**, *261*, 189–203, and references therein. 1,4-diazabutadienes: For a "classical" review see: h) G. van Koten, K. Vrieze, *Adv. Organomet. Chem.* **1982**, *21*, 151–239; for the recent use of dad in stabilizing low-valent [16 + 1] Nb and Ta complexes, see: i) P. J. Daff, M. Etienne, B. Donnadieu, S. Z. Knottenbelt, J. E. McGrady, *J. Am. Chem. Soc.* **2002**, *124*, 3818–3819, and references therein.

[2] For a recent example of redox isomerism involving Cu^{2+}(L^{2-})/Cu$^+$(L$^{\bullet-}$) see: a) J. Rall, M. Wanner, M. Albrecht, F. M. Hornung, W. Kaim, *Chem. Eur. J.* **1999**, *5*, 2802–2809, and references therein; for redox isomerism involving Rh^{2+}(L^{2-})/Rh$^+$(L$^{\bullet-}$) see: b) G. A. Abakumov, G. A. Razuvaev, V. I. Nevodchikov, V. K. Cherkasov, *J. Organomet. Chem.* **1988**, *341*, 485–494.

[3] Rh and Ir NHchel complexes were electrochemically generated;[1b–g] however, only black oligomeric compounds such as [Rh^0(phen)$_2$]$_x$ could be isolated.[1b] Stacking to give oligomeric units through metal–metal bonds has been reported also for 9,10-phenanthroquinonediiminerhodium and -iridium complexes: S.-S. Chern, G.-H. Lee, S.-M. Peng, *J. Chem. Soc. Chem. Commun.* **1994**, 1645, and references therein.

[4] See the discussion about addressing the problem of assigning the redox state in the dad complexes [Ir^{3+}Cp*Cl(dad^0)]PF$_6$ and [Ir^{+3}Cp*(dad^{2-})] and citing previous work in the field; S. Berger, F. Baumann, T. Scheiring, W. Kaim, *Z. Anorg. Allg. Chem.* **2001**, *627*, 620–630.

[5] a) H. Schönberg, S. Boulmaâz, M. Wörle, L. Liesum, A. Schweiger, H. Grützmacher, *Angew. Chem.* **1998**, *109*, 1492; *Angew. Chem. Int. Ed.* **1998**, *37*, 1423; b) H. Grützmacher, H. Schönberg, S. Boulmaâz, M. Mlakar, S. Deblon, S. Loss, M. Wörle, *J. Chem. Soc. Chem. Commun.* **1998**, 2623; c) S. Deblon, L. Liesum, J. Harmer, H. Schönberg, A. Schweiger, H. Grützmacher, *Chem. Eur. J.* **2002**, *8*, 601.

[6] For the synthesis of **3** as intermediate for *N*-heterocyclic carbenes see: C. Böhler, D. Stein, N. Donati, H. Grützmacher, *New. J. Chem.* **2002**, *26*, 1291 – 1295.

[7] Structure of **6**: crystals from dichloromethane/*n*-hexane; $C_{33}H_{24}N_2O_3F_3SRh$, orthorhombic, *P*bca; $a = 16.681(1)$, $b = 13.156(1)$, $c = 25.905(2)$ Å; $V = 5685.0(7)$ Å^3; $Z = 8$; $\rho_{calcd} = 1.609$ g cm^{-3}; crystal dimensions: $0.35 \times 0.16 \times 0.01$; diffractometer: Bruker SMART APEX CCD area detector; $Mo_{K\alpha}$ radiation, 100 K, $2\Theta_{max} = 50.32^\circ$; 32594 reflections, 5054 independent ($R_{int} = 0.0565$), direct methods; refinement against full-matrix (versus F^2) with SHELXTL (Version 5.1) and SHELXL-97, 388 parameters, 6 restraints, $R1 = 0.072$ and w$R2$ (all data) $= 0.192$, max/min residual electron density: $1.10/-1.34 \times 10^{30}$ e m^{-3}. CCDC-205265 contains the supplementary crystallographic data for this paper. These data can be obtained free of charge via www.ccdc.cam.ac.uk/conts/retrieving.html (or from the Cambridge Crystallographic Data Centre, 12 Union Road, Cambridge CB2 1EZ, UK; fax: (+44) 1223-336-033; or e-mail: deposit@ccdc.cam.ac.uk).

[8] Pentacoordinate complexes have been reported; for recent examples see: a) P. J. Daff, M. Etienne, B. Donnadieu, S. Z. Knottenbelt, J. E. McGrady, *J. Am. Chem. Soc.* **2002**, *124*, 3818 – 3819, and references therein; b) L. Gonsalvi, J. A. Gaunt, H. Adams, A. Castro, G. J. Sunley, A. Haynes, *Organometallics* **2003**, *22*, 1047 – 1054.

[9] A. Schweiger, G. Jeschke, *Principles of Pulse Electron Paramagnetic Resonance*, Oxford Press, **2001**.

[10] a) C. Lee, W. Yang, R. G. Parr, *Phys. Rev.* **1988**, *B 37*, 785; b) A. D. Becke, *J. Chem. Phys.* **1993**, *98*, 5648; c) C. Adamo, V. Barone, *J. Chem. Phys.* **1996**, *101*, 664.

[11] G.Jeschke, A. Schweiger, *J. Chem. Phys.* **1997**, *106*, 9979.

[12] M. L. Munzarová, P. Kubáèek, M. Kaupp, *J. Am. Chem. Soc.* **2002**, *122*, 11900.

[13] M. Munzarová, M. Kaupp, *J. Phys. Chem. A* **1999**, *103*, 9966.

[14] I. Gromov, J. Shane, J. Forrer, R. Rakhmatoullin, Y. Rozentzwaig, A. Schweiger, *J. Magn. Reson.* **2001**, *149*, 196.

[15] G. Jeschke, R. Rakhmatullin, A. Schweiger, *J. Magn. Reson.* **1998**, *131*, 261.

[16] see web site: http://www.esr.ethz.ch

[17] Z. Madi, S. Van Doorslaer, A. Schweiger, *J. Magn. Reson.* **2002**, *154*, 181.

Received: December 23, 2002 [F4700]